HHS Public Access

Author manuscript

Dev Biol. Author manuscript; available in PMC 2018 September 01.

Published in final edited form as:

Dev Biol. 2017 September 01; 429(1): 132–146. doi:10.1016/j.ydbio.2017.06.037.

Differential requirement of SUFU in tissue development discovered in a hypomorphic mouse model

Maria A. Hoelzl[1,*], **Karin Heby-Henricson**[1], **Marco Gerling**[1], **José M. Dias**[3], **Raoul V. Kuiper**[2], **Cornelius Trünkle**[1], **Åsa Bergström**[1], **Johan Ericson**[3], **Rune Toftgård**[1], and **Stephan Teglund**[1,**]

[1]Department of Biosciences and Nutrition, Karolinska Institutet, SE-141 83 Huddinge, Sweden

[2]Department of Laboratory Medicine, Karolinska Institutet, SE-141 86 Huddinge, Sweden

[3]Department of Cell and Molecular Biology, Karolinska Institutet, SE-171 77 Stockholm, Sweden

Abstract

Suppressor of Fused (SUFU) is an essential negative regulator of the Hedgehog (HH) pathway and involved in GLI transcription factor regulation. Due to early embryonic lethality of *Sufu*$^{-/-}$ mice, investigations of SUFU's role later in development are limited to conditional, tissue-specific knockout models. In this study we developed a mouse model (*Sufu*$^{Ex456(fl)/Ex456(fl)}$) with hypomorphic features where embryos were viable up to E18.5, although with a spectrum of developmental defects of varying severity, including polydactyly, exencephaly and omphalocele. Development of certain tissues, like the skeleton, was more affected than that of others such as skin, which remained largely normal. Interestingly, no apparent changes in the dorso-ventral patterning of the neural tube at E9.0 could be seen. Thus, this model provides an opportunity to globally study SUFU's molecular function in organogenesis beyond E9.5. Molecularly, *Sufu*$^{Ex456(fl)/Ex456(fl)}$ embryos displayed aberrant mRNA splicing and drastically reduced levels of *Sufu* wild-type mRNA and SUFU protein in all tissues. As a consequence, at E9.5 the levels of all three different GLI proteins were reduced. Interestingly, despite the reduction of GLI3 protein levels, the critical ratio of the GLI3 full-length transcriptional activator versus GLI3 truncated repressor remained unchanged compared to wild-type embryos. This suggests that the limited amount of SUFU protein present is sufficient for GLI processing but not for stabilization. Our data demonstrate that tissue development is differentially affected in response to the reduced SUFU levels, providing novel insight regarding the requirements of different levels of SUFU for proper organogenesis.

Keywords

Hedgehog pathway; Suppressor of Fused; GLI; Hypomorph; Embryogenesis; Skeletogenesis

[*]Corresponding author. Tel.: +46 8 52481064. maria.holzl@ki.se. [**]Corresponding author. Tel.: +46 8 52481157. stephan.teglund@ki.se.

INTRODUCTION

The Hedgehog (HH) signaling pathway is a key regulatory signaling cascade, critical for embryonic development and stem cell maintenance (Briscoe and Thérond, 2013; Hui and Angers, 2011). Perturbations of the pathway during embryogenesis cause developmental defects such as holoprosencephaly (Roessler et al., 1996) and polydactyly (Zhulyn and Hui, 2015). Postnatal misactivation is firmly linked to different types of cancer such as medulloblastoma and basal cell carcinoma (Teglund and Toftgård, 2010). Main components of the HH pathway comprise the receptor Patched1 (PTCH1), which in its unbound state inhibits the receptor Smoothened (SMO), preventing downstream signaling. In this repressed state, Suppressor of fused (SUFU), located downstream of SMO, binds to the GLI (GLI1 through 3) transcription factors, impeding target gene transcription. Binding of any of the three HH ligands Sonic, Indian, or Desert Hedgehog (SHH, IHH, or DHH) to PTCH1 results in downstream pathway activation through SMO de-repression followed by dissociation of the SUFU-GLI complexes and initiation of target gene transcription (Briscoe and Thérond, 2013; Humke et al., 2010; Pak and Segal, 2016; Tukachinsky et al., 2010). HH signal transduction is closely coupled to the primary cilium, a microtubule-based organelle present on most mammalian cells, the integrity of which is necessary for normal pathway function (Goetz et al., 2009).

Studies in mice established SUFU as a major negative regulator of the HH pathway as SUFU deficiency results in embryonic lethality around E9.5 and is associated with aberrant HH activity (Cooper et al., 2005; Svärd et al., 2006). SUFU is able to bind to all three GLI transcription factors and regulates their activity in various ways (Cheng and Bishop, 2002; Dunaeva et al., 2003; Kogerman et al., 1999; Merchant et al., 2004; Stone et al., 1999; C. Wang et al., 2010). While GLI2 and GLI3 are the primary effectors in the pathway, GLI1 acts as an amplifier of the signal and is itself a target gene of the pathway (Grindley et al., 1997; Hynes et al., 1997; Lee et al., 1997). Additionally, as opposed to GLI1, GLI2 and GLI3 exist as both activating full-length (FL) as well as shorter repressor (R) proteins (Dai et al., 1999; Sasaki et al., 1999). However, GLI2 mainly acts as activator and has a negligible role as repressor, whereas GLI3 mainly functions as repressor rather than activator (Bai et al., 2002; Ding et al., 1998; Matise et al., 1998; Sasaki et al., 1997; B. Wang et al., 2000). The right balance of GLI repressive and activating signals is critical for the output of proper HH pathway activity. SUFU here plays a key role in regulating GLI stabilization and processing and thus considerably contributes to maintaining accurate HH signaling (Chen et al., 2009; Humke et al., 2010; Jia et al., 2009; Lin et al., 2014; Makino et al., 2015; C. Wang et al., 2010).

Studies on conditional *Sufu* knockout in mice have provided insight into effects of complete loss of SUFU in various types of tissues such as skin (Z. J. Li et al., 2012), lung (Lin et al., 2014) and bone (Hsu et al., 2011). Although these studies further emphasize the importance of SUFU as a crucial negative modulator of the pathway, they provide limited information on dose-dependent regulation through SUFU. In this study we generated a novel *Sufu* mutant allele ($Sufu^{Ex456(fl)/Ex456(fl)}$), enabling us to explore the impact of significantly reduced SUFU levels on HH pathway activity globally in all tissue types. We show that $Sufu^{Ex456(fl)/Ex456(fl)}$ embryos displayed congenital anomalies including exencephaly, cleft

lip and palate and omphalocele. Furthermore, we demonstrate that while skin development and early dorsal-ventral patterning of the neural tube overall remained largely unaffected, skeletal patterning and development was severely impaired. Our results provide novel information regarding the requirement for SUFU for pathway inhibition, revealing differential, tissue-specific sensitivity towards diminished SUFU levels.

MATERIALS AND METHODS

Generation of the targeting construct and the conditional *Sufu* mutant allele

The conditional *Sufu* mutant mouse strain, B6;129X1-*Sufu*^{tm2Rto}, accession number MGI: 5888725 (initially labeled *Sufu*$^{neo(frt)Ex456(fl)}$), harboring loxP sites flanking exon 4 – 6, was created by standard gene targeting techniques. To generate the targeting construct we used the pDELBOY-3X conditional targeting vector (a kind gift from T. Mäkelä, the Haartman Institute, University of Helsinki, Finland) containing a PGK-*neo* resistance cassette flanked by *frt* sites for positive selection, two *loxP* sites, and a herpes simplex virus (HSV) thymidine kinase (TK) cassette for negative selection. A 1.3 kb fragment of the *Sufu* gene, spanning exons 4, 5 and 6, was generated by PCR from a 14.1 kb XbaI fragment spanning a region between *Sufu* intron 3 and intron 8 of the BAC clone 17985 from the mouse 129X1/SvJ ESC BAC library II (Genome Systems, Inc.). The PCR primers F1 and R1 (see Suppl. Table 1 for primer sequences) were flanked by AccI sites that enabled subcloning of the fragment (exons 4, 5 and 6) into ClaI, positioned in-between the two loxP sites in pDELBOY-3X.. The left and right arms of homology, 2.0 kb and 3.5 kb respectively, were cloned into the same vector on either side of PGK-*neo*. The targeting construct was linearized and electroporated into the RW4 embryonic stem cell (ESC) line (129X1/SvJ mouse strain) placed under neo/G418 selection, essentially according to (Svärd et al., 2006). One of approximately 900 clones that survived the positive-negative selection had undergone homologous recombination, as detected and verified by Southern blot analysis (data not shown). The correctly targeted 129X1/SvJ ESCs (clone 3C4) were injected into B6D2F1 morulas, which were implanted into CD1 pseudopregnant females to generate chimeras. For germline transmission of the mutant *Sufu* allele, male chimeras were bred to C57BL/6J females to generate heterozygous F1 offspring.

Mouse strains and animals used

Sufu$^{neo(frt)Ex456(fl)/+}$ mice were crossed to Tg(ACTFLP-L)Dym (Dymecki, 1996) to eliminate the PGK-neomycin resistance cassette (PGK-*neo*). The resulting B6;129X1-*Sufu*$^{tm2.1Rto}$ mice, accession number MGI:58887123, hereafter named *Sufu*$^{Ex456(fl)/+}$, were initially on a mixed B6;129 background with continuous backcrossing to C57BL/6J during the time of the study. As *Sufu*$^{Ex456(fl)/+}$ mice appeared phenotypically normal they were, together with wild-type mice, used as controls. The B6;FVB-Tg(EIIa-cre)*C5379Lmgd* mouse strain was a kind gift from L. Holmgren, Karolinska Institutet (Lakso et al., 1996) and was crossed with *Sufu*$^{Ex456(fl)}$ to generate B6;129X1-*Sufu*$^{tm2.2Rto}$ offspring, hereafter named *Sufu*$^{\Delta}$. The *Sufu* knockout strain B6.129X1-*Sufu*^{tm1Rto} (*Sufu*$^{-/-}$) was as previously described (Svärd et al., 2006). BALB/c nude spontaneous mutant mice (strain C.Cg/AnBomTac-Foxn1^{nu} N20; Charles River) and NOD/SCID (NOD.CB17/AlhnRj-*Prkdc*^{scid}/j) were used for skin grafts as described below. All mice were housed in an SPF barrier facility

according to local and national regulations and the study was approved by the Stockholm South Animal Ethics Committee.

Genotyping

For PCR genotyping, DNA was prepared from ear-punch biopsies or yolk sacs according to the HotSHOT method (Truett et al., 2000). For the *Sufu*$^{Ex456(fl)}$ PCR genotyping assays both mutant and wild-type *Sufu* alleles were detected using the following primer: Intr3 F1, Intr4 R1, and pgkNeo R1 before; and Intr3 F2, Ex6 F1, and Intr6 R3 after *in vivo* excision of PGK-*neo* (see Suppl. Table 1 for primer sequences). Genotyping of *Sufu*$^{+/-}$ mice was performed as previously described (Svärd et al., 2006).

RNA isolation and quantitative real-time PCR

RNA was extracted using either the Qiagen RNeasy Kit (E9.5 embryos) or the Qiagen AllPrepDNA/RNA/Protein Kit (E16.5 tissues) according to manufacturer's protocol. Complementary DNA (cDNA) synthesis, qRT-PCR as well as analysis were performed as described previously (Hoelzl et al., 2015). At least three independent experiments were performed where each reaction was measured in triplicates. *Arbp*, *Hsp90*, and *Gapdh* were used as reference genes and gave comparable results. Outcomes are presented as fold change relative to wild-type, and mean values ± SEM of three independent experiments are displayed. Primer sequences are listed in Suppl. Table 1.

Detection of mRNA variants, cloning and sequencing

RNA isolation from E9.5 embryos or E16.5 tissues with subsequent cDNA synthesis was performed as described above. Primers located in exon 2 and exon 7 (Ex2Ex7; see Suppl. Table 1 for primer sequences) together with either the Platinum® *Taq* DNA Polymerase High Fidelity or the AmpliTaq Gold® DNA Polymerase (both Invitrogen) were used to amplify the loxP-flanked region ranging from exon 4 through exon 6. The resulting PCR products were separated on an agarose gel and photographed using the Gel Doc 2000 imaging system (BioRad). PCR products from E9.5 embryos were extracted from the gel and purified applying the QIAquick Gel Extraction Kit (Qiagen), followed by sequencing using the Ex2Ex7 primers. Alternatively, PCR fragments were cloned into the pCR™4-TOPO® TA sequencing vector using the TOPO TA Cloning® Kit (Invitrogen) and sequenced with the included M13 primer.

Yolk sac DNA from E9.5 embryos was amplified using Platinum® *Taq* DNA Polymerase High Fidelity (Invitrogen) with the primer pairs Intron3F2 and Intron6R3, or MSF5-6 F (located in intron 4) and MSF5-6 R (located in intron 6) (Suppl. Table 1). The resulting PCR product was loaded on an agarose gel, purified using QIAquick Gel Extraction Kit (Qiagen) and sent for sequencing (Eurofins Genomics).

Protein extraction and western blotting

For each experiment, three E9.5 embryos of the same genotype were pooled and lysed using RIPA buffer (50 mM Tris, 150 mM NaCl, 1% NP-40, 0.5% sodium deoxycholate, 0.1% SDS) complemented with 1 mM PMSF and a protease inhibitor mixture (cOmplete, EDTA-free, Roche). For the downstream application, 15–40 μg protein of whole embryo lysate was

used. For E16.5 tissue, the Qiagen AllPrepDNA/RNA/Protein Kit was applied and samples were directly analyzed by SDS-PAGE without prior protein quantification. Proteins were separated on 7.5%–12% Mini-PROTEAN® TGX™ Precast Gels (Bio-Rad) and transferred to nitrocellulose membranes (Amersham) prior to incubation with the following primary Antibodies directed against: GLI1 (V812, #2534, Cell Signaling, 1:1000); GLI2 (AF3635, R&D Systems, 1:500); GLI3 (AF3690, R&D Systems, 1:1000); SUFU (C81H7, #2522, Cell Signaling, 1:500; H300, sc-28847, Santa Cruz Biotechnology, 1:500), Calnexin (C-20, sc-6465, Santa Cruz Biotechnology, 1:1000), β-actin (clone AC-15, A5441, Sigma-Aldrich, 1:20 000), and Vinculin (Clone hVIN-1, V9131, Sigma-Aldrich, 1:10 000). Antibody binding was detected using IRD680- and IRD800-labelled secondary antibodies (LI-COR) and the membranes were scanned on a LI-COR Odyssey CLx imaging system. Quantitative analysis was performed using Image Studio (LI-COR), and outcomes are presented as mean values ± SEM of at least three independent experiments.

Skin grafts

Dorsal skin from E18.5 $Sufu^{Ex456(fl)/Ex456(fl)}$ (n=4) and control (n=3) embryos was transplanted onto the back of adult BALB/c nude spontaneous mutant mice (strain C.Cg/AnBomTac-Foxn1^{nu} N20; Charles River) or NOD/SCID (NOD.CB17/AlhnRj-$Prkdc^{scid}$/j). After 14 weeks, animals were sacrificed and skin grafts, with surrounding recipient skin, were harvested. The tissue was fixated in 4% PFA overnight followed by embedding, sectioning, and hematoxylin and eosin staining.

Skin permeability assay and skeletal staining

Assessment of the embryonic (E14.5, E17.5 and E18.5) skin barrier status by staining with 5-bromo-4-chloro-3-indolyl-β-D-galactopyranoside (X-gal) as well as skeletal staining of E16.5 and E18.5 embryos using Alcian Blue/Alizarin Red were performed as described previously (Norum et al., 2015).

Immunohistochemistry

Immunohistochemical staining on formalin-fixed, paraffin-embedded (FFPE) tissue sections was performed as described previously (Hoelzl et al., 2015). Briefly, tissue was harvested and fixed in 4% PFA overnight, followed by embedding and sectioning. The following primary antibodies were applied: Phospho-Histone H3 (Ser10, #9701, Cell Signaling, 1:1000), Ki67 (NCL-Ki67p, Leica Biosystems, 1:3000), Trp63 (4A4, sc-8431, Santa Cruz Biotechnology, 1:500), K5 (PRB-160P, Covance, 1:5000), K14 (PRB-155P, Covance, 1:5000), K10 (PRB-159P, Covance, 1:1000), Loricrin (PRB-145P, Covance, 1:200), and alpha-SMA (ab5694, Abcam, 1:500). Analysis of air space and lung tissue was conducted using the Pannoramic MIDI scanner and HistoQuant software (both 3DHISTECH). For assessing neural tube patterning, E9.0 embryos were fixed in 4% PFA for 3 hours or overnight and subsequently immersed in 30% sucrose solution before embedding in Tissue-Tek® OCT (optimal cutting temperature) solution. Samples were cryo-sectioned at 12 μm thickness and incubated with the following primary antibodies: Nkx2.2 (74.5A5, DSHB, 1:20), Pax6 (HPA030775, Sigma, 1:1000), Olig2 (AB9610, Millipore, 1:1000), FoxA2 (4C7, DSHB, 1:10), and Nkx6.1 (F65A2, DSHB, 1:100). Alexa Fluor secondary antibodies (Invitrogen) were used for detection with the Zeiss LSM880 laser-scanning microscope.

Micro-computed tomography (μCT)

For 3D whole embryo and bone imaging using μCT, E18.5 embryos were fixed in 4% PFA overnight and then stored in PBS. μCT was performed with a Quantum FX μCT imaging system (Caliper Life Sciences, Perkin Elmer, Inc.), 3D rendering of DICOM data was done in OsiriX, v.5.5.2 (Rosset et al., 2004).

Statistical analysis

Statistical analysis was performed using Prism 6.0 (GraphPad Software, Inc., La Jolla, CA). For assessing differences between two samples, *t*-test was applied and for three or more samples, one-way ANOVA was used.

RESULTS

Targeting of *Sufu* exons 4-5-6 results in a mutant with hypomorphic features

Sufu knockout ($Sufu^{-/-}$) mice die in utero around embryonic day 9.5 (E9.5) with severe cephalic deformations including an open fore-, mid-, and hindbrain and neural tube (Svärd et al., 2006). Therefore, we aimed to create a conditional allele by standard gene targeting techniques in mouse embryonic stem cells (ESCs), by introducing two *loxP* sites flanking a region including exons 4, 5, and 6 (Suppl. Figure 1A). After the initial gene targeting, the resulting conditional allele $Sufu^{neo(frt)Ex456(fl)}$ also contained a neomycin resistance cassette (PGK-*neo*) in intron 3 which was flanked by *frt* sites. $Sufu^{neo(frt)Ex456(fl)/+}$ mice were crossed to Flp deleter mice (Dymecki, 1996) to eliminate PGK-neo *in vivo* by Flp-mediated recombination, resulting in $Sufu^{Ex456(fl)/+}$ mice. Heterozygotes carrying the conditional allele were viable and fertile and phenotypically indistinguishable from wild-type mice. The functionality of the novel conditional allele was confirmed by crossing of $Sufu^{Ex456(fl)/+}$ mice to the *EIIa-cre* deleter strain ((Lakso et al., 1996)), achieving recombination in the one-cell embryo. The resulting $Sufu^{\Delta/+}$ mice harbored a deletion of the desired floxed region as verified by genotyping PCR (data not shown), and appeared normal in phenotype. As expected, homozygous $Sufu^{\Delta/\Delta}$ mice died around E9.5 and resembled the $Sufu^{-/-}$ phenotype. Intercrossing of $Sufu^{Ex456(fl)/+}$ mice, to generate homozygotes, did surprisingly not result in viable $Sufu^{Ex456(fl)/Ex456(fl)}$ offspring, despite the absence of a *Cre* allele that could drive recombination (Suppl. Figure 1B; 0/111 pups). To test whether the Flp-mediated excision of the PGK-neo cassette has had a negative impact on the conditional allele, we intercrossed heterozygous mice still harboring the neomycin cassette. As no homozygous pups were obtained also in this case, we excluded possible negative effects of the Flp-mediated recombination as underlying cause of the unexpected lack of viable pups.

To explore whether $Sufu^{Ex456(fl)}$ homozygotes resembled $Sufu^{-/-}$ mice, we isolated E9.5 embryos. $Sufu^{Ex456(fl)/Ex456(fl)}$ embryos frequently displayed, compared to controls (Figure 1A), modest cephalic defects in the midbrain region (Figure 1D). As the embryos otherwise were morphologically similar to controls, we concluded that the phenotype of our $Sufu^{Ex456(fl)}$ allele does not correspond to a complete elimination of the *Sufu* gene suggesting a partial loss of gene product and/or activity consistent with a hypomorphic allele.

Homozygosity for the *Sufu*$^{Ex456(fl)}$ allele leads to multiple developmental defects and perinatal lethality

To further dissect the consequences of our mutant allele, we isolated *Sufu*$^{Ex456(fl)/Ex456(fl)}$ embryos at various developmental stages between E9.5 and E18.5. As heterozygotes and wild-type embryos were phenotypically identical, they served as interchangeable controls. *Sufu*$^{Ex456(fl)/Ex456(fl)}$ embryos were viable until E18.5 but showed severe defects throughout all stages of development (Figures 1D–F, 1J–L, 1N–N′ and 1P), which became more obvious with increasing age of the embryo. Although pups homozygous for the mutant allele were born, no live *Sufu*$^{Ex456(fl)/Ex456(fl)}$ offspring was found at postnatal day 1. Developmental abnormalities, quantified for embryos at E18.5, included cleft lip and palate (25/26; 96.2%), exencephaly (7/26; 26.9%), polydactyly (26/26; 100%), hematoma (24/26; 92.3%) and omphalocele (25/26; 96.2%). Furthermore, we frequently observed macroglossia as well as a severely impaired eye development in these embryos. In conclusion, the fact that *Sufu*$^{Ex456(fl)/Ex456(fl)}$ embryos survived beyond E9.5 further supported the interpretation that targeting of *Sufu* exons 4, 5 and 6 resulted in a mutant allele with hypomorphic characteristics. Furthermore, the results implied that while reduced amount and/or activity of SUFU protein suffices to ensure adequate development of vital organs up E18.5, it is incompatible with viable pups postnatally.

A point mutation in a putative 3′ splice regulatory site in the *Sufu*$^{Ex456(fl)}$ allele as possible cause of aberrant transcripts

To shed light onto the underlying cause of the hypomorphic characteristics of the novel mutant allele, we sequenced the cDNA from mRNA of E9.5 *Sufu*$^{Ex456(fl)/Ex456(fl)}$ embryos using primers located in exons 2 and 7, spanning the critically targeted exons 4 through 6. We detected one single cDNA band in wild-type controls. *Sufu*$^{Ex456(fl)/Ex456(fl)}$ embryos, on the other hand, harbored two additional novel variants, which appeared shorter in size (Figure 2A). In addition to whole embryo lysates, the occurrence of these truncated variants was confirmed in various tissues of E16.5 embryos (Suppl. Figure 2). Sequence analysis revealed that these transcripts were lacking either both exon 5 and exon 6 (*SufuΔEx5-6*) or exon 6 alone (*SufuΔEx6*) but otherwise did not show any sequence divergence from wild-type mRNA (Figure 2A and data not shown). Elimination of exon 6 resulted in a frame-shift, creating a premature stop codon in exon 7, which would lead to a hypothetical shortened protein of 26.8 kDa. The *SufuΔEx5-6* variant maintains the reading frame and would theoretically generate a protein of slightly smaller size (48.2 kDa) compared to wild-type SUFU (54 kDa).

To fathom possible factors accounting for the identified splice variants found in *Sufu*$^{Ex456(fl)/Ex456(fl)}$ embryos, we sequenced genomic DNA using primers located outside the *loxP* sites in intron 3 and intron 6. We discovered two point mutations (G→A and T→A [Figures 2B and 2C]) in intron 5, of which one (T→A) was predicted to be located in a putative 3′ mRNA splice regulatory site using the online SROOGLE splicing regulatory sequence detection tool (Schwartz et al., 2009). As we could not detect other mutations, it is likely that these newly discovered point mutations were responsible for the identified novel *SufuΔEx5-6* and *SufuΔEx6* transcripts and that they probably represent artifacts introduced during the construct generation.

No increased hedgehog target gene activation in E9.5 *Sufu*$^{Ex456(fl)/Ex456(fl)}$ embryos despite reduced *Sufu* mRNA and protein levels

Given the severe developmental defects in *Sufu*$^{Ex456(fl)/Ex456(fl)}$ embryos we reasoned that the additional *Sufu* mRNA variants were possibly generated on the expense of wild-type transcripts, which in turn could lead to a reduction of SUFU protein and thus disturbed processing of GLI-FL into GLI-R as well as overall increased HH pathway activity. Using primers exclusively detecting *Sufu* wild-type transcripts, we found an approximately 10-fold decrease of wild-type mRNA in *Sufu*$^{Ex456(fl)/Ex456(fl)}$ E9.5 embryos (Figure 3A). Consequently, we discovered drastically diminished levels of SUFU full-length protein amounting to approximately only a fifth of wild-type levels (Figure 3B). Regarding the possibility that the *SufuΔEx5-6* and/or *SufuΔEx6* transcripts would generate protein products of the calculated sizes 48.2 kDa and 26.8 kDa, respectively, the two different SUFU antibodies used in this study did not reveal any such isoforms (Figure 3B and data not shown). The monoclonal antibody used in Figure 3B is raised towards a peptide surrounding Alanine 340 and would be present in the 48.2 kDa putative protein. The other, polyclonal antibody used is specific for amino acids 185–484 and partly encompasses sequences present in both the 48.2 kDa and 26.8 kDa isoforms. However, only the 54 kDa full-length SUFU protein could be seen in either case.

Embryos lacking SUFU (*Sufu*$^{-/-}$) exhibit a constitutive activation of the HH pathway (Svärd et al., 2006) and served as a control. As *Sufu* mRNA and SUFU protein levels were severely reduced in *Sufu*$^{Ex456(fl)/Ex456(fl)}$ mice, we presumed that there would be an increase in HH pathway signaling activity. Thus, we analyzed mRNA expression levels of known target genes, indicative of active HH signaling. Contrary to our expectations, none of the HH target genes, including *Gli1* and *Ptch1,* showed increased expression in the *Sufu*$^{Ex456(fl)/Ex456(fl)}$ embryos compared to wild-type (Figure 3C). In fact, one of the target genes, *FoxA2*, instead showed a statistically significant decrease (Figure 3C). As expected, *Sufu*$^{-/-}$ controls displayed an augmented expression of HH target genes compared to wild-type. The HH target gene *FoxA2* itself positively regulates expression of *Shh* (Jeong, 2003), and in line with this *Sufu*$^{-/-}$ embryos displayed significantly higher levels of *Shh* mRNA (Figure 3D). However, no change in *Shh* expression was detected in embryos harboring the *Sufu*$^{Ex456(fl)}$ allele. Levels of *Smo* were comparable in embryos of all three genotypes (Figure 3D). *Gli2* and *Gli3* mRNA expression in *Sufu*$^{Ex456(fl)/Ex456(fl)}$ embryos were unaltered (Figure 3D), which is in contrast to the significant reduction of *Gli3* expression in *Sufu*$^{-/-}$ embryos (Figure 3D).

Although we did not find changes in *Gli2* and *Gli3* gene expression in *Sufu*$^{Ex456(fl)/Ex456(fl)}$ E9.5 embryos we suspected, due to the overt malformations, consequences of the reduced SUFU levels on GLI protein stabilization and/or processing. Western blot analysis at E9.5 revealed a stark decline of GLI1 in *Sufu*$^{Ex456(fl)/Ex456(fl)}$ embryos (Figure 4A). GLI2 levels were also strongly reduced (Figure 4B) and GLI3FL and GLI3R levels were significantly decreased in *Sufu*$^{Ex456(fl)/Ex456(fl)}$ embryos compared to wild-type (Figure 4C). Remarkably however, the GLI3FL/GLI3R ratio was not strongly affected (Figure 4C). We further found a significant reduction in the amount of GLI2, GLI3FL and GLI3R in embryos completely devoid of SUFU, corroborating previous data (Chen et al., 2009; Humke et al., 2010; Jia et

al., 2009; Kise et al., 2009; C. Wang et al., 2010). Additionally, the GLI3FL/GLI3R ratio was increased in $Sufu^{-/-}$ and $Sufu^{\Delta/\Delta}$ embryos (Figure 4C), supporting a mechanism in which GLI3FL is insufficiently processed in the absence of SUFU. Our data back the concept that SUFU is central for stabilization of GLI2 and GLI3FL and further suggest that even the low levels of SUFU seen here suffice for promoting efficient processing of GLI3FL to generate GLI3R.

Severe skeletal malformations in $Sufu^{Ex456(fl)/Ex456(fl)}$ mice

HH signaling plays an important role during bone development (Koziel et al., 2005; Miao et al., 2004; St-Jacques et al., 1999; Zeller et al., 2009) and SUFU has been demonstrated to act as a negative regulator of the pathway during chondrocyte differentiation and limb development (Hsu et al., 2011; J. Li et al., 2015; Zhulyn and Hui, 2015; Zhulyn et al., 2014). We used micro-computed tomography (μCT; Suppl. Videos 1A and 1B) and alcian blue/alizarin red staining (Figures 5A–U and 6A–R) to analyze bone development at E16.5 and E18.5. $Sufu^{Ex456(fl)/Ex456(fl)}$ embryos were characterized by distinct skeletal and craniofacial abnormalities as can be seen in Figures 5 and 6. We observed decreased bone density of the skull bones (Figure 5K) as well as clefting of the nasal region (nasal bone and capsule) and the frontal bone (Figure 5L and 5M). In addition, $Sufu^{Ex456(fl)/Ex456(fl)}$ embryos had truncated mandibles, lacked the supraoccipital bone, showed hypoplasia of parietal and interparietal bone structures and disorganized cervical vertebrae (Figures 5K, O and 5T). We also found a deficit in bone ossification in femora, tibiae as well as humeri, radii and ulnae, whereas fibulae and scapulae were not significantly affected (Figures 6D, E, and 6I, J). Additionally, $Sufu^{Ex456(fl)/Ex456(fl)}$ embryos displayed polydactyly in both fore- and hindlimbs and showed a pronounced plantar flexion of the hindlimb (Figures 6D, I, P and 6R). At E16.5 ossification of the metacarpals and metatarsals was barely noticeable in $Sufu^{Ex456(fl)/Ex456(fl)}$ embryos, and calcification of phalanges was absent in both control and $Sufu^{Ex456(fl)/Ex456(fl)}$ mice at this age (Figures 6K, M, O and 6Q). Analysis of HH target gene expression at E16.5 showed comparable levels of *Ptch1*, *Hhip* and *Gli1* in front- and hindpaw whereas *Gli2* and *Gli3* were significantly upregulated (Suppl. Figures 3B–F). Levels of GLI2 protein in $Sufu^{Ex456(fl)/Ex456(fl)}$ paws were higher compared to wild-type (Suppl. Figure 4C) whereas the GLI3FL/GLI3R ratio was not significantly altered. At E18.5, control animals showed ossification in fore- and hindlimb autopods to a similar extent (Figures 6L and 6N). On the contrary, mineralization in $Sufu^{Ex456(fl)/Ex456(fl)}$ autopods was only detected in metatarsals as well as in the distal forelimb phalanges and occasionally in metacarpals (Figures 6P and 6R). Although the number of ribs did not differ from that in controls, they were misshapen and in some cases branching (Figures 5D and 6C). Additionally, we noticed that the sternum was split (Figure 5S) and that the pelvis of $Sufu^{Ex456(fl)/Ex456(fl)}$ embryos showed reduced ossification of the pubic bone (Figure 5U). Our data demonstrate that insufficient levels of SUFU resulted in improper bone development despite overall unchanged GLI3FL/GLI3R ratio as early as at E9.5.

Skin development is not compromised in $Sufu^{Ex456(fl)/Ex456(fl)}$ embryos but skin changes appear in aged $Sufu^{Ex456(fl)/+}$ mice

HH signaling plays a pivotal role in skin and hair follicle (HF) development (Mill, 2003; St-Jacques et al., 1998), and over-activation of the pathway results in basal cell carcinomas

(Teglund and Toftgård, 2010). Previous studies reported that deletion of *Sufu* in the K5 compartment of the skin compromised normal skin and HF development (Z. J. Li et al., 2012). Microscopic analysis of the phenotype of $Sufu^{Ex456(fl)/Ex456(fl)}$ mice did not reveal any differences in the number or developmental stages of HFs at E16.5 (data not shown) or E18.5 (Figure 7B). Whereas *Gli1* mRNA and GLI1 protein were reduced at E16.5 in $Sufu^{Ex456(fl)/Ex456(fl)}$ skin (Suppl. Figures 3D and 4B), other HH target genes such as *Ptch1* and *Hhip* were comparable to wild-type (Suppl. Figures 3B and 3C). *Gli2* expression was upregulated (Suppl. Figure 3E) but protein levels remained unchanged (Suppl. Figure 4C). *Gli3* mRNA was not significantly changed (Suppl. Figure 3F) and the GLI3FL/GLI3R ratio was unaltered (Suppl. Fig 4D). The basal cell layer, visualized by Keratin 14 and Keratin 5 staining (Figures 7S and 7T) (Moll et al., 2008), displayed a normal one-layer thickness and staining for the proliferation markers Ki67 and phospho-Histone H3 (Figures 7K and 7L) did not reveal any difference in proliferation. Expression of TRP63 (Figure 7R), involved in the stratification processes of the skin (Barbieri and Pietenpol, 2006), was normal and no difference could be detected in the supra-basal (K10) and cornified ($Loricrin^{+}$) layers (Figures 7U and 7V). In line with our observations, no defect in the establishment of skin barrier function could be detected (Figures 7F–H). Hence, we were unable to detect a skin phenotype in $Sufu^{Ex456(fl)/Ex456(fl)}$ embryos, despite their severe developmental defects in bone development.

As mice homozygous for the $Sufu^{Ex456(fl)}$ allele die around birth, we transplanted skin of E18.5 embryos onto immunocompromised mice to be able to uncover possible long-term effects of SUFU reduction on skin development. Previous studies have shown that transplants of *Sufu*-deficient embryonic skin or deletion of *Sufu* in the epidermis of adult mice resulted in epidermal hyperplasia (Z. J. Li et al., 2012). Control and $Sufu^{Ex456(fl)/Ex456(fl)}$ skin grafts were analyzed after a period of 14 weeks to provide enough time for the hair follicles to undergo multiple hair cycles. A small patch of hair was observed about 2 weeks after transplantation independent of genotype, demonstrating that the severe reduction of SUFU levels did not impair outgrowth of hair (Suppl. Figures 5A–B′). The epidermis of $Sufu^{Ex456(fl)/Ex456(fl)}$ allografts was comparable to control transplants and did not show any signs of hyperplasia 14 weeks post transplantation (Suppl. Figures 5C and 5D). We furthermore did not observe any obvious defects in stratification and hair follicles developed normally. Our data indicate that the significant reduction of SUFU protein found in our $Sufu^{Ex456(fl)}$ model is, as opposed to complete loss, not sufficient to compromise epidermal differentiation or cause hyperproliferation in embryonic skin and skin transplants.

As we reported previously for $Sufu^{-/+}$ mice, a reduction of SUFU levels results in basaloid skin changes, slowly progressing as the mice age and are generally apparent around 1.5–2 years of age (Svärd et al., 2006). To investigate whether the heterzygous $Sufu^{Ex456(fl)}$ mice also develop similar changes in the aging skin, mice heterozygous for the $Sufu^{Ex456(fl)}$ allele were analyzed at 24 months of age and compared to $Sufu^{-/+}$ animals. Confirming our previous findings, ventral skin, paw and tail of $Sufu^{-/+}$ control mice showed typical lesions including basaloid follicular hamartoma (BFH) and epidermal hyperplasia (Suppl. Figures 6A–C). Interestingly, we also detected hyperplastic areas as well as BFHs in the epidermis of $Sufu^{Ex456(fl)/+}$ animals, though to a much lesser extent and smaller in size (Suppl. Figures 6D–F). Furthermore, BFHs were restricted to the ventral epidermis whereas they were also

found in *Sufu*$^{-/+}$ paw and tail skin. The lower frequency of BFHs in *Sufu*$^{Ex456(fl)/+}$ animals compared to *Sufu*$^{-/+}$ mice is thus in line with the presence of a hypomorphic allele.

Dorso-ventral patterning of the neural tube remains unaffected in *Sufu*$^{Ex456(fl)/Ex456(fl)}$ mice

The fundamental role of HH signaling for neural tube patterning is well established (Briscoe and Ericson, 2001; Dessaud et al., 2008), and deletion of *Sufu* results in a loss of dorsal neuronal cell-type identity and ventralization of the neural tube (Svärd et al., 2006). We explored the possibility of patterning defects in the E9.0 *Sufu*$^{Ex456(fl)/Ex456(fl)}$ neural tube and compared to *Sufu*$^{-/-}$ and wild-type embryos. In concordance with previous reports (Svärd et al., 2006) we found that FOXA2, a marker for floor plate cells (Placzek and Briscoe, 2005), was misexpressed along the dorso-ventral axis in the *Sufu*$^{-/-}$ neural tube (Figure 8O). In contrast, no such alteration was observed in *Sufu*$^{Ex456(fl)/Ex456(fl)}$ embryos (Figure 8N). Likewise, while the expression of the ventral transcription factors OLIG2, NKX2.2 and NKX6.1 was expanded into dorsal regions in *Sufu*$^{-/-}$ embryos (Figures 8F, I and 8L) (Svärd et al., 2006), *Sufu*$^{Ex456(fl)/Ex456(fl)}$ and wild-type neural tubes showed a comparable expression pattern (Figures 8D, E, 8G, H, 8J, K, and 8M, N). Additionally, PAX6 expression in the dorsal neural tube was not affected in *Sufu*$^{hypo/hypo}$ (Figure 8B), but *Sufu*$^{-/-}$ embryos (Figure 8C). Taken together these data demonstrate that levels of SUFU in the *Sufu*$^{Ex456(fl)/Ex456(fl)}$ neural tube are sufficient to ensure accurate cell-type specification along its dorso-ventral axis at this stage.

Disturbed lung development and omphalocele formation in *Sufu*$^{Ex456(fl)/Ex456(fl)}$ mice

HH signaling is centrally involved in lung organogenesis (Bellusci et al., 1997; Motoyama et al., 1998) and complete loss of *Sufu* impairs lung myofibroblast development (Lin et al., 2014). Given that skin development as well as neural tube patterning were unaffected in *Sufu*$^{Ex456(fl)/Ex456(fl)}$ embryos, we sought to investigate if moderately reduced levels of SUFU were essential for proper development and morphogenesis of the lung. We analyzed lungs of *Sufu*$^{Ex456(fl)/Ex456(fl)}$ embryos at various developmental stages and could not detect any phenotypic difference between controls and *Sufu*$^{Ex456(fl)/Ex456(fl)}$ embryos at E13.5 and E15.5 (Figures 9A, B and 9D, E). Analysis of HH target genes at E16.5 revealed a significant downregulation of *Gli1* mRNA in lungs of *Sufu*$^{Ex456(fl)/Ex456(fl)}$ embryos (Suppl. Fig 3D) whereas GLI1 protein remained relatively unchanged (Suppl. Fig 4B). Expression of *Ptch1*, *Hhip* as well as *Gli2* and *Gli3* was not significantly affected (Suppl. Figures 3B, C and 3E, F), and GLI2 and GLI3 protein levels did not show any significant difference compared to wild-type (Suppl. Figures 4C and 4D). At E18.5 lungs from *Sufu* hypomorphic mice displayed smaller alveoli and the interstitial mesenchyme lining the air sacs appeared to be thicker (Figure 9F). Furthermore, we found a significant reduction of alveolar-space in favor of lung tissue in *Sufu*$^{Ex456(fl)/Ex456(fl)}$ embryos supporting the idea for a role for SUFU in alveolar development during later embryonic development (Figures 9G and 9H). Myofibroblast differentiation is reduced in lungs devoid of SUFU (Lin et al., 2014), yet α-SMA staining did not reveal any obvious differences between *Sufu*$^{Ex456(fl)/Ex456(fl)}$ and control lungs, and α-SMA^{+} cells were predominantly found in cells surrounding bronchioles and blood vessels (Suppl. Figures 7A and 7B). Together, our data indicate that reduced levels of SUFU lead to a disorganization of lung saccules, but do not impair development of bronchiolar smooth muscle and blood vessels.

HH signaling has further been demonstrated to be involved in ventral body wall formation and aberrantly increased signaling levels to be a causative factor for omphalocele formation (Matsumaru et al., 2011). During midgestation, starting at E12.5, the visceral organs herniate out of the torso into the umbilical cord, due to the limiting space of the peritoneal cavity. This normal physiological process occurs transiently and is completely reversed by E16.5. In control mice, the protrusion of embryonic viscera was detected from E12.5 on and was completely recovered by E16.5, leaving only the umbilical cord outside the abdomen (Suppl. Figures 8A–C and Suppl. Video 2A). In stark contrast, 96% of $Sufu^{Ex456(fl)/Ex456(fl)}$ embryos continued to display umbilical herniation at E18.5 (Suppl. Figure 8F and Suppl. Video 2B), indicating that a certain level of SUFU protein restricting HH signaling is required to ensure proper body wall closure.

DISCUSSION

In this study, we generated a novel mouse model with hypomorphic features, in which the SUFU full-length protein levels were drastically reduced, but not absent, in all tissues studied. As a result, the embryos extend their viability from around E9.5 in a complete *Sufu* loss-of-function mutant to around birth for this $Sufu^{Ex456(fl)/Ex456(fl)}$ mutant, thereby opening up the possibility to analyze affected tissues farther into development. The cause of the reduced SUFU protein levels is likely a direct consequence of a similar reduction of the corresponding *Sufu* wild-type transcript caused by aberrant mRNA splicing. Qualitatively, this splicing pattern was present in all embryonic tissues analyzed supporting a general effect not specific to certain tissues, revealing that different tissues possess differential sensitivities towards limiting SUFU amounts as discussed below.

The *SufuΔEx5-6* and *SufuΔEx6* transcripts could hypothetically generate novel SUFU protein isoforms. An alternative explanation for the observed phenotype of the $Sufu^{Ex456(fl)/Ex456(fl)}$ embryos other than a mere reduction of the full-length SUFU protein would be that these isoforms possess alternative functions, for example acting as dominant-negative proteins. However, we were unable to detect any such variants suggesting that if they are produced, they may possibly be unstable and thus rapidly degraded. Another observation speaking against the notion that there could be functionally relevant SUFU protein isoforms with alternative functions is the fact the heterozygous $Sufu^{Ex456(fl)}$ embryos do not display any overt phenotypic aberrations. In addition, aged heterozygous $Sufu^{Ex456(fl)}$ mutant mice develop a similar, but milder, skin phenotype as the previously described heterozygous *Sufu* knockout mice (Svärd et al., 2006).

HH signaling is crucial for patterning and outgrowth of the limb (Zeller et al., 2009) and complete loss of SUFU perturbs digit patterning due to a block in GLI3R formation (Zhulyn et al., 2014; Zhulyn and Hui, 2015). $Sufu^{Ex456(fl)/Ex456(fl)}$ embryos exhibit polydactyly and we show that ossification in long bones of both fore- and hindlimb was affected in E18.5 embryos. However, in contrast to embryos with complete absence of SUFU, $Sufu^{Ex456(fl)/Ex456(fl)}$ did not display severe hypoplasia (J. Li et al., 2015; Zhulyn and Hui, 2015). Forelimb autopods show great reduction or even absence of ossification at E16.5 and E18.5 consistent with previous findings (J. Li et al., 2015; Zhulyn and Hui, 2015). Hindlimb autopods show no ossification at E16.5 but do so later in the metatarsals at E18.5 indicating

that reduced SUFU levels rather cause a delay than complete block in hindlimb ossification. Interestingly, at E16.5 there are very subtle changes in the amounts and ratio of GLI3FL and GLI3R in $Sufu^{Ex456(fl)/Ex456(fl)}$ fore- and hindlimbs compared to wild-type controls. Only the forelimb shows a small but significant reduction in the amount of GLI3R, which would correlate with the more pronounced phenotype of the forelimb. Taken together, this suggests a differential spatio-temporal role for SUFU in fore- and hindlimb development.

Complete loss of *Sufu* specifically in the skin impairs epidermal differentiation and results in basaloid follicular hamartoma (Z. J. Li et al., 2012). In contrast, the reduction of SUFU as present here in the $Sufu^{Ex456(fl)/Ex456(fl)}$ mouse is not sufficient to induce apparent changes in the epidermis up until death occurs around term. Furthermore, neither could we observe any obvious skin or hair defects when $Sufu^{Ex456(fl)/Ex456(fl)}$ embryonic skin allografts were grown on immunodeficient mice for 14 weeks. We speculate that in the skin, as opposed to bone, lower levels of SUFU are sufficient to maintain proper pathway control or that additional factors such as Kif7 compensate for reduced SUFU levels (Z. J. Li et al., 2012). This possibility is also supported by the observation that GLI2 protein levels in E16.5 skin are similar as in wild-type, in contrast to E16.5 limbs. As $Sufu^{Ex456(fl)/+}$ mice age, however, the skin shows mild hyperplasia, although less frequent and in a less severe form than appears in $Sufu^{-/+}$ mice (Svärd et al., 2006). Thus, the effect of moderately reduced SUFU levels on skin homeostasis becomes evident only at advanced age.

Deletion of *Sufu* results in ectopic expression of ventral markers along the dorso-ventral axis and loss of dorsal cell-type specification in the ventral neural tube (Svärd et al., 2006) at E9.0–E9.5. Despite the low SUFU levels observed in the $Sufu^{Ex456(fl)/Ex456(fl)}$ embryos, neural tube patterning was not affected in these embryos, indicating that the overall balance between GLI activators and repressors is maintained at this stage.

In the lung we see a defect on alveolar maturation as the $Sufu^{Ex456(fl)/Ex456(fl)}$ are getting close to term at E18.5. Previous studies of a lung-specific, *Dermo1-Cre* driven, *Sufu* knockout mouse model revealed a more severe phenotype including a smaller overall lung size and reduced branching morphogenesis in addition to the alveolar phenotype seen here (Lin et al., 2014). Again, as in the other $Sufu^{Ex456(fl)/Ex456(fl)}$ E16.5 tissues studied, there is no increased HH pathway activity detected as assessed by *Ptch1*, *Hhip*, and *Gli1* target gene expression. On the contrary, as in skin, we found a significant downregulation of *Gli1* mRNA. It is possible that the lung alveolar defect and reduction in lung alveolar space is a main contributor to lethality at birth, as we could not recover any live $Sufu^{Ex456(fl)/Ex456(fl)}$ pups at P1.

In humans, an omphalocele is a relatively rare closure defect of the abdominal wall occurring in approximately 1/4000 live births (Sadler, 2010). The etiology behind the malformation is not fully understood but appears to be heterogeneous. Based on mouse models, HH signaling has been implicated in omphalocele formation in a HH signal time- and dose-dependent manner (Matsumaru et al., 2011). Interestingly, $Sufu^{Ex456(fl)/Ex456(fl)}$ embryos fail to recover the physiological umbilical herniation by E16.5 ending up with an omphalocele at term, indicating that SUFU plays a role in preventing omphalocele

pathogenesis. To our knowledge there is no study in humans directly linking the HH pathway to the disease but it could be an interesting avenue for further exploration.

The morphological abnormalities observed, such as limb and craniofacial defects indicate compromised GLI3R function (Hui and Joyner, 1993). At E9.5 we observed a reduction in the amounts of GLI3FL, GLI2 and GLI3R, although to a lesser extent than in *Sufu*$^{-/-}$ embryos (Chen et al., 2009; Humke et al., 2010; Jia et al., 2009; Kise et al., 2009; C. Wang et al., 2010). The reduction of GLI3FL and GLI2 corroborates SUFU's established role in stabilization of these GLI proteins. As GLI3R is a product of GLI3FL processing, the concomitant reduction in the amount of GLI3R seen in the *Sufu*$^{Ex456(fl)/Ex456(fl)}$ embryos could thus possibly be explained by simple stoichiometry. This explanation is also supported by the interesting fact that the GLI3 FL/R ratio in the *Sufu*$^{Ex456(fl)/Ex456(fl)}$ remained the same as in wild-type embryos, which is in stark contrast to the situation in *Sufu*$^{-/-}$ embryos where the ratio is strongly skewed towards the GLI3FL. Hence we conclude that the reduced level of SUFU protein limits the amount of GLI3FL it can sequester, but does not seem to affect the normal GLI3FL processing rate. This view assumes that the GLI3R turnover rate remains unchanged. The situation here is in contrast to complete loss of SUFU where both processing and stabilization are affected.

Intriguingly, despite the distinct phenotypes in the *Sufu*$^{Ex456(fl)/Ex456(fl)}$ embryos indicating an ectopically activated HH pathway and a significant reduction in the absolute amounts of GLI3R, at E9.5 there is no increase in the expression of any of the five HH target genes *Gli1*, *Ptch1*, *Ptch2*, *Hhip*, or *FoxA2* analyzed. On the contrary, there is even a slight but significant reduction in *FoxA2* expression. This is very different in E9.5 *Sufu*$^{-/-}$ embryos where there is a ~1.5-3.5-fold increase in the expression of these target genes. Thus, merely the amounts and ratio of GLI activators/repressors and the resulting target gene expression in the *Sufu*$^{Ex456(fl)/Ex456(fl)}$ E9.5 embryos are seemingly not enough to explain the developmental phenotypes indicative of ectopic pathway activation and our results hence point to further complexity in HH pathway regulation. Also, Western Blot and qRT-PCR analysis of E16.5 *Sufu*$^{Ex456(fl)/Ex456(fl)}$ tissues did not show any clear and consistent indication of overactive pathway either. However, due to analyses of whole tissues, upregulation in a small, but critical cell population may have been masked.

Previously, a *Sufu* hypomorphic mouse model was described where a missense mutation resulted in a threonine to isoleucine substitution at amino acid residue 396 (T396I) (Makino et al., 2015). Similar to what was seen in our *Sufu*$^{Ex456(fl)/Ex456(fl)}$ model, embryos were not viable and showed comparable morphological phenotypes. One major difference between their model and ours, however, is that the T396I mutation only affected SUFU's role in regulating and processing of GLI3FL but did not influence GLI2 or GLI1.

CONCLUSION

In this study, we have developed a novel *Sufu* mutant mouse model with hypomorphic features, characterized by overall reduced levels of full-length SUFU mRNA and protein. Our data showed that embryos homozygous for the *Sufu*$^{Ex456(fl)}$ allele were viable up to E18.5, but displayed severe developmental defects including polydactyly, exencephaly, and

omphalocele. We have demonstrated that diminished SUFU levels resulted in variable tissue specific responses, as skin and early neural tube patterning remained largely unaffected, while bone development was severely impaired. Our *Sufu*$^{Ex456(fl)}$ mouse model provides a novel tool to investigate how SUFU regulates GLI processing and stability, and how different tissue-specific requirements of SUFU levels balances GLI activator/repressor function and consequently HH pathway activity.

Supplementary Material

Refer to Web version on PubMed Central for supplementary material.

Acknowledgments

We thank the Karolinska Center for Transgene Technologies (KCTT) particularly B.-M. Skog and G. Brolin, as well as E. Tüksammel for technical assistance. This work was supported by the Swedish Research Council (S.T.), the Swedish Cancer Society and NIH/NCI MMHCC (R.T.), the Robert Lundberg Memorial Foundation (M.A.H and K.H-H.), the German Research Foundation (DFG GE 2386/1-1 [M.G.]) and the Swedish Cancer Foundation (Cancerfonden, 2014/1376 [M.G.]).

ABBREVIATIONS

GLI	glioma associated protein
HH	hedgehog
Hypo	hypomorph
SUFU	suppressor of fused

References

Bai CB, Auerbach W, Lee JS, Stephen D, Joyner AL. Gli2, but not Gli1, is required for initial Shh signaling and ectopic activation of the Shh pathway. Development. 2002; 129:4753–4761. [PubMed: 12361967]

Barbieri CE, Pietenpol JA. p63 and epithelial biology. Experimental Cell Research. 2006; 312:695–706. DOI: 10.1016/j.yexcr.2005.11.028 [PubMed: 16406339]

Bellusci S, Furuta Y, Rush MG, Henderson R, Winnier G, Hogan BL. Involvement of Sonic hedgehog (Shh) in mouse embryonic lung growth and morphogenesis. Development. 1997; 124:53–63. [PubMed: 9006067]

Briscoe J, Ericson J. Specification of neuronal fates in the ventral neural tube. Curr Opin Neurobiol. 2001; 11:43–49. [PubMed: 11179871]

Briscoe J, Thérond PP. The mechanisms of Hedgehog signalling and its roles in development and disease. Nat Rev Mol Cell Biol. 2013; 14:416–429. DOI: 10.1038/nrm3598 [PubMed: 23719536]

Chen MH, Wilson CW, Li YJ, Law KKL, Lu CS, Gacayan R, Zhang X, Hui CC, Chuang PT. Cilium-independent regulation of Gli protein function by Sufu in Hedgehog signaling is evolutionarily conserved. Genes & Development. 2009; 23:1910–1928. DOI: 10.1101/gad.1794109 [PubMed: 19684112]

Cheng SY, Bishop JM. Suppressor of Fused represses Gli-mediated transcription by recruiting the SAP18-mSin3 corepressor complex. Proc Natl Acad Sci USA. 2002; 99:5442–5447. DOI: 10.1073/pnas.082096999 [PubMed: 11960000]

Cooper AF, Yu KP, Brueckner M, Brailey LL, Johnson L, McGrath JM, Bale AE. Cardiac and CNS defects in a mouse with targeted disruption of suppressor of fused. Development. 2005; 132:4407–4417. DOI: 10.1242/dev.02021 [PubMed: 16155214]

Dai P, Akimaru H, Tanaka Y, Maekawa T, Nakafuku M, Ishii S. Sonic Hedgehog-induced activation of the Gli1 promoter is mediated by GLI3. Journal of Biological Chemistry. 1999; 274:8143–8152. [PubMed: 10075717]

Dessaud E, McMahon AP, Briscoe J. Pattern formation in the vertebrate neural tube: a sonic hedgehog morphogen-regulated transcriptional network. Development. 2008; 135:2489–2503. DOI: 10.1242/dev.009324 [PubMed: 18621990]

Ding Q, Motoyama J, Gasca S, Mo R, Sasaki H, Rossant J, Hui CC. Diminished Sonic hedgehog signaling and lack of floor plate differentiation in Gli2 mutant mice. Development. 1998; 125:2533–2543. [PubMed: 9636069]

Dunaeva M, Michelson P, Kogerman P, Toftgård R. Characterization of the physical interaction of Gli proteins with SUFU proteins. J Biol Chem. 2003; 278:5116–5122. DOI: 10.1074/jbc.M209492200 [PubMed: 12426310]

Dymecki SM. Flp recombinase promotes site-specific DNA recombination in embryonic stem cells and transgenic mice. Proc Natl Acad Sci USA. 1996; 93:6191–6196. [PubMed: 8650242]

Goetz, SC., Ocbina, PJR., Anderson, KV. Primary Cilia, Methods in Cell Biology. Elsevier; 2009. The Primary Cilium as a Hedgehog Signal Transduction Machine; p. 199-222.

Grindley JC, Bellusci S, Perkins D, Hogan BL. Evidence for the involvement of the Gli gene family in embryonic mouse lung development. Developmental Biology. 1997; 188:337–348. DOI: 10.1006/dbio.1997.8644 [PubMed: 9268579]

Hoelzl MA, Heby-Henricson K, Bilousova G, Rozell B, Kuiper RV, Kasper M, Toftgård R, Teglund S. Suppressor of Fused Plays an Important Role in Regulating Mesodermal Differentiation of Murine Embryonic Stem Cells In Vivo. Stem Cells and Development. 2015; 24:2547–2560. DOI: 10.1089/scd.2015.0050 [PubMed: 26176320]

Hsu SHC, Zhang X, Yu C, Li ZJ, Wunder JS, Hui CC, Alman BA. Kif7 promotes hedgehog signaling in growth plate chondrocytes by restricting the inhibitory function of Sufu. Development. 2011; 138:3791–3801. DOI: 10.1242/dev.069492 [PubMed: 21795282]

Hui C-C, Angers S. Gli Proteins in Development and Disease. Annu Rev Cell Dev Biol. 2011; 27:513–537. DOI: 10.1146/annurev-cellbio-092910-154048 [PubMed: 21801010]

Hui CC, Joyner AL. A mouse model of greig cephalopolysyndactyly syndrome: the extra-toesJ mutation contains an intragenic deletion of the Gli3 gene. Nat Genet. 1993; 3:241–246. DOI: 10.1038/ng0393-241 [PubMed: 8387379]

Humke EW, Dorn KV, Milenkovic L, Scott MP, Rohatgi R. The output of Hedgehog signaling is controlled by the dynamic association between Suppressor of Fused and the Gli proteins. Genes & Development. 2010; 24:670–682. DOI: 10.1101/gad.1902910 [PubMed: 20360384]

Hynes M, Stone DM, Dowd M, Pitts-Meek S, Goddard A, Gurney A, Rosenthal A. Control of cell pattern in the neural tube by the zinc finger transcription factor and oncogene Gli-1. Neuron. 1997; 19:15–26. [PubMed: 9247260]

Jeong Y. Distinct regulators of Shh transcription in the floor plate and notochord indicate separate origins for these tissues in the mouse node. Development. 2003; 130:3891–3902. DOI: 10.1242/dev.00590 [PubMed: 12835403]

Jia J, Kolterud Å, Zeng H, Hoover A, Teglund S, Toftgård R, Liu A. Suppressor of Fused inhibits mammalian Hedgehog signaling in the absence of cilia. Developmental Biology. 2009; 330:452–460. DOI: 10.1016/j.ydbio.2009.04.009 [PubMed: 19371734]

Kise Y, Morinaka A, Teglund S, Miki H. Sufu recruits GSK3beta for efficient processing of Gli3. Biochem Biophys Res Commun. 2009; 387:569–574. DOI: 10.1016/j.bbrc.2009.07.087 [PubMed: 19622347]

Kogerman P, Grimm T, Kogerman L, Krause D, Undén AB, Sandstedt B, Toftgard R, Zaphiropoulos PG. Mammalian suppressor-of-fused modulates nuclear-cytoplasmic shuttling of Gli-1. Nat Cell Biol. 1999; 1:312–319. DOI: 10.1038/13031 [PubMed: 10559945]

Koziel L, Wuelling M, Schneider S, Vortkamp A. Gli3 acts as a repressor downstream of Ihh in regulating two distinct steps of chondrocyte differentiation. Development. 2005; 132:5249–5260. DOI: 10.1242/dev.02097 [PubMed: 16284117]

Lakso M, Pichel JG, Gorman JR, Sauer B, Okamoto Y, Lee E, Alt FW, Westphal H. Efficient in vivo manipulation of mouse genomic sequences at the zygote stage. Proc Natl Acad Sci USA. 1996; 93:5860–5865. [PubMed: 8650183]

Lee J, Platt KA, Censullo P, Ruiz i Altaba A. Gli1 is a target of Sonic hedgehog that induces ventral neural tube development. Development. 1997; 124:2537–2552. [PubMed: 9216996]

Li J, Wang Q, Cui Y, Yang X, Li Y, Zhang X, Qiu M, Zhang Z, Zhang Z. Suppressor of Fused Is Required for Determining Digit Number and Identity via Gli3/Fgfs/Gremlin. PLoS ONE. 2015; 10:e0128006.doi: 10.1371/journal.pone.0128006 [PubMed: 26001200]

Li ZJ, Nieuwenhuis E, Nien W, Zhang X, Zhang J, Puviindran V, Wainwright BJ, Kim PCW, Hui CC. Kif7 regulates Gli2 through Sufu-dependent and -independent functions during skin development and tumorigenesis. Development. 2012; 139:4152–4161. DOI: 10.1242/dev.081190 [PubMed: 23034632]

Lin C, Chen MH, Yao E, Song H, Gacayan R, Hui CC, Chuang PT. Differential regulation of Gli proteins by Sufu in the lung affects PDGF signaling and myofibroblast development. Developmental Biology. 2014; 392:324–333. DOI: 10.1016/j.ydbio.2014.05.014 [PubMed: 24886827]

Makino S, Zhulyn O, Mo R, Puviindran V, Zhang X, Murata T, Fukumura R, Ishitsuka Y, Kotaki H, Matsumaru D, Ishii S, Hui CC, Gondo Y. T396I mutation of mouse Sufu reduces the stability and activity of Gli3 repressor. PLoS ONE. 2015; 10:e0119455.doi: 10.1371/journal.pone.0119455 [PubMed: 25760946]

Matise MP, Epstein DJ, Park HL, Platt KA, Joyner AL. Gli2 is required for induction of floor plate and adjacent cells, but not most ventral neurons in the mouse central nervous system. Development. 1998; 125:2759–2770. [PubMed: 9655799]

Matsumaru D, Haraguchi R, Miyagawa S, Motoyama J, Nakagata N, Meijlink F, Yamada G. Genetic Analysis of Hedgehog Signaling in Ventral Body Wall Development and the Onset of Omphalocele Formation. PLoS ONE. 2011; 6:e16260.doi: 10.1371/journal.pone.0016260.g006 [PubMed: 21283718]

Merchant M, Vajdos FF, Ultsch M, Maun HR, Wendt U, Cannon J, Desmarais W, Lazarus RA, de Vos AM, de Sauvage FJ. Suppressor of fused regulates Gli activity through a dual binding mechanism. Molecular and Cellular Biology. 2004; 24:8627–8641. DOI: 10.1128/MCB.24.19.8627-8641.2004 [PubMed: 15367681]

Miao D, Liu H, Plut P, Niu M, Huo R, Goltzman D, Henderson JE. Impaired endochondral bone development and osteopenia in Gli2-deficient mice. Experimental Cell Research. 2004; 294:210–222. DOI: 10.1016/j.yexcr.2003.10.021 [PubMed: 14980515]

Mill P. Sonic hedgehog-dependent activation of Gli2 is essential for embryonic hair follicle development. Genes & Development. 2003; 17:282–294. DOI: 10.1101/gad.1038103 [PubMed: 12533516]

Moll R, Divo M, Langbein L. The human keratins: biology and pathology. Histochem Cell Biol. 2008; 129:705–733. DOI: 10.1007/s00418-008-0435-6 [PubMed: 18461349]

Motoyama J, Liu J, Mo R, Ding Q, Post M, Hui CC. Essential function of Gli2 and Gli3 in the formation of lung, trachea and oesophagus. Nat Genet. 1998; 20:54–57. DOI: 10.1038/1711 [PubMed: 9731531]

Norum JH, Bergström Å, Andersson AB, Kuiper RV, Hoelzl MA, Sørlie T, Toftgård R. A conditional transgenic mouse line for targeted expression of the stem cell marker LGR5. Developmental Biology. 2015; 404:35–48. DOI: 10.1016/j.ydbio.2015.05.002 [PubMed: 26003047]

Pak E, Segal RA. Hedgehog Signal Transduction: Key Players, Oncogenic Drivers, and Cancer Therapy. Developmental Cell. 2016; 38:333–344. DOI: 10.1016/j.devcel.2016.07.026 [PubMed: 27554855]

Placzek M, Briscoe J. The floor plate: multiple cells, multiple signals. Nat Rev Neurosci. 2005; 6:230–240. DOI: 10.1038/nrn1628 [PubMed: 15738958]

Roessler E, Belloni E, Gaudenz K, Jay P, Berta P, Scherer SW, Tsui LC, Muenke M. Mutations in the human Sonic Hedgehog gene cause holoprosencephaly. Nat Genet. 1996; 14:357–360. DOI: 10.1038/ng1196-357 [PubMed: 8896572]

Rosset A, Spadola L, Ratib O. OsiriX: an open-source software for navigating in multidimensional DICOM images. J Digit Imaging. 2004; 17:205–216. DOI: 10.1007/s10278-004-1014-6 [PubMed: 15534753]

Sadler TW. The embryologic origin of ventral body wall defects. Semin Pediatr Surg. 2010; 19:209–214. DOI: 10.1053/j.sempedsurg.2010.03.006 [PubMed: 20610194]

Sasaki H, Hui C, Nakafuku M, Kondoh H. A binding site for Gli proteins is essential for HNF-3beta floor plate enhancer activity in transgenics and can respond to Shh in vitro. Development. 1997; 124:1313–1322. [PubMed: 9118802]

Sasaki H, Nishizaki Y, Hui C, Nakafuku M, Kondoh H. Regulation of Gli2 and Gli3 activities by an amino-terminal repression domain: implication of Gli2 and Gli3 as primary mediators of Shh signaling. Development. 1999; 126:3915–3924. [PubMed: 10433919]

Schwartz S, Hall E, Ast G. SROOGLE: webserver for integrative, user-friendly visualization of splicing signals. Nucleic Acids Res. 2009; 37:W189–92. DOI: 10.1093/nar/gkp320 [PubMed: 19429896]

St-Jacques B, Dassule HR, Karavanova I, Botchkarev VA, Li J, Danielian PS, McMahon JA, Lewis PM, Paus R, McMahon AP. Sonic hedgehog signaling is essential for hair development. Current Biology. 1998; 8:12–12. DOI: 10.1016/S0960-9822(98)70443-9

St-Jacques B, Hammerschmidt M, McMahon AP. Indian hedgehog signaling regulates proliferation and differentiation of chondrocytes and is essential for bone formation. Genes & Development. 1999; 13:2072–2086. [PubMed: 10465785]

Stone DM, Murone M, Luoh S, Ye W, Armanini MP, Gurney A, Phillips H, Brush J, Goddard A, de Sauvage FJ, Rosenthal A. Characterization of the human suppressor of fused, a negative regulator of the zinc-finger transcription factor Gli. Journal of Cell Science. 1999; 112(Pt 23):4437–4448. [PubMed: 10564661]

Svärd J, Henricson KH, Persson-Lek M, Rozell B, Lauth M, Bergström Å, Ericson J, Toftgård R, Teglund S. Genetic Elimination of Suppressor of Fused Reveals an Essential Repressor Function in the Mammalian Hedgehog Signaling Pathway. Developmental Cell. 2006; 10:187–197. DOI: 10.1016/j.devcel.2005.12.013 [PubMed: 16459298]

Teglund S, Toftgård R. Hedgehog beyond medulloblastoma and basal cell carcinoma. Biochimica et Biophysica Acta (BBA) - Reviews on Cancer. 2010; 1805:181–208. DOI: 10.1016/j.bbcan.2010.01.003 [PubMed: 20085802]

Truett GE, Heeger P, Mynatt RL, Truett AA, Walker JA, Warman ML. Preparation of PCR-quality mouse genomic DNA with hot sodium hydroxide and tris (HotSHOT). Biotech. 2000; 29:52–54.

Tukachinsky H, Lopez LV, Salic A. A mechanism for vertebrate Hedgehog signaling: recruitment to cilia and dissociation of SuFu-Gli protein complexes. The Journal of Cell Biology. 2010; 191:415–428. DOI: 10.1083/jcb.201004108 [PubMed: 20956384]

Wang B, Fallon JF, Beachy PA. Hedgehog-regulated processing of Gli3 produces an anterior/posterior repressor gradient in the developing vertebrate limb. Cell. 2000; 100:423–434. [PubMed: 10693759]

Wang C, Pan Y, Wang B. Suppressor of fused and Spop regulate the stability, processing and function of Gli2 and Gli3 full-length activators but not their repressors. Development. 2010; 137:2001–2009. DOI: 10.1242/dev.052126 [PubMed: 20463034]

Zeller R, Lopez-Rios J, Zuniga A. Vertebrate limb bud development: moving towards integrative analysis of organogenesis. Nat Rev Genet. 2009; 10:845–858. DOI: 10.1038/nrg2681 [PubMed: 19920852]

Zhulyn O, Hui C-C. Sufu and Kif7 in limb patterning and development. Dev Dyn. 2015; 244:468–478. DOI: 10.1002/dvdy.24249 [PubMed: 25581370]

Zhulyn O, Li D, Deimling S, Vakili NA, Mo R, Puviindran V, Chen M-H, Chuang P-T, Hopyan S, Hui C-C. A Switch from Low to High Shh Activity Regulates Establishment of Limb Progenitors and Signaling Centers. Developmental Cell. 2014; doi: 10.1016/j.devcel.2014.03.002

HIGHLIGHTS

- Generation of a *Sufu* mutant allele with hypomorphic characteristics.
- *Sufu*$^{Ex456(fl)/Ex456(fl)}$ embryos show diminished levels of SUFU full-length protein.
- *Sufu*$^{Ex456(fl)/Ex456(fl)}$ mutants survive up to E18.5.
- Bone, but not skin or early neural tube patterning is affected in Sufu$^{Ex456(fl)/Ex456(fl)}$ embryos.

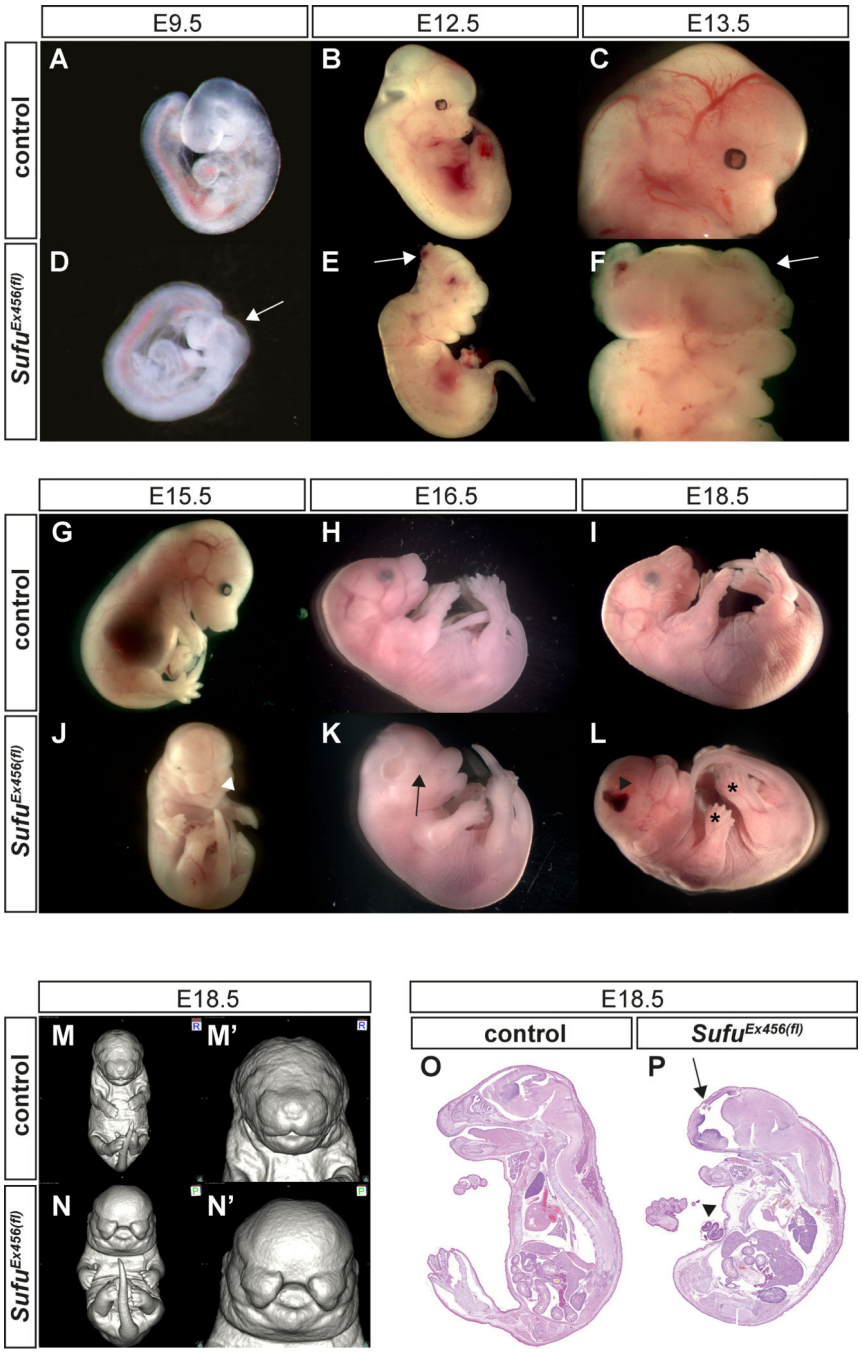

Fig. 1. Severe developmental defects in *Sufu*$^{Ex456(fl)/Ex456(fl)}$ embryos

(A–L) Display of morphological phenotypes of embryos of indicated genotype and age showing developmental malformations in *Sufu*$^{Ex456(fl)/Ex456(fl)}$ embryos compared to controls. White arrow, cephalic abnormalities; white arrowhead, cleft lip and palate; black arrow, location of eye; asterisk, polydactyly; black arrowhead, hematoma. (M–N′) μCT 3D surface rendering of E18.5 *Sufu*$^{Ex456(fl)/Ex456(fl)}$ and control embryos emphasizing the cleft lip phenotype in animals homozygous for the *Sufu*$^{Ex456(fl)}$ allele. (O–P) Hematoxylin and

eosin stained sagittal sections of E18.5 embryos displaying brain abnormalities (arrow) and omphalocele (arrowhead) in the mutant embryos.

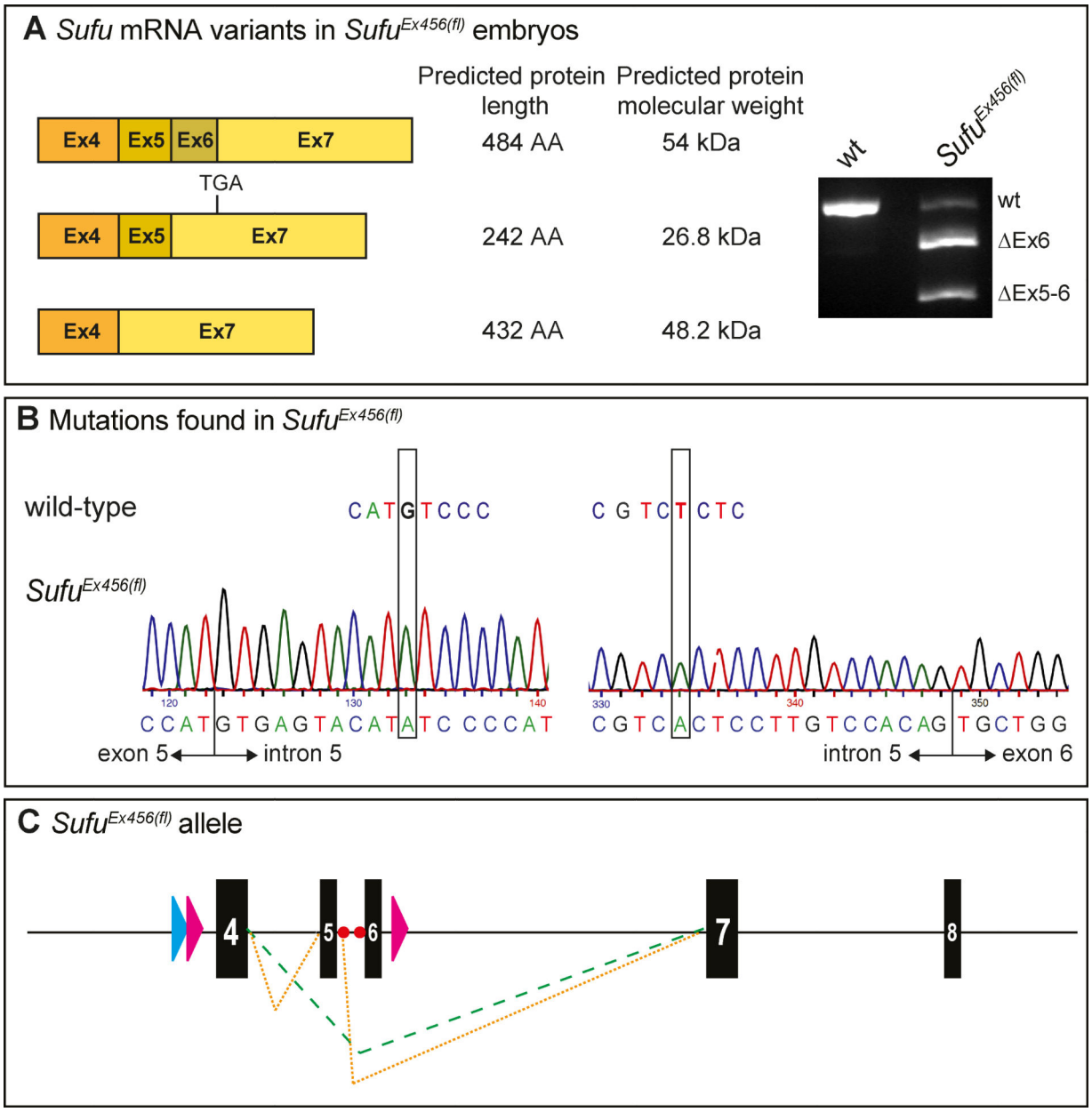

Fig. 2. Identification of aberrant *Sufu* transcripts and point mutations in *Sufu*$^{Ex456(fl)/Ex456(fl)}$ embryos

(A) Cartoon (left) and RT-PCR agarose gel analysis (right) of detected transcripts in *Sufu* mutant embryos and predicted length and molecular weight of hypothetical protein products. *Sufu* exon 6 skipping (ΔEx6) leads to a frame-shift in the coding region creating a premature stop codon (TGA) in exon 7. wt, wild-type. (B) Sequence showing the discovered point mutations (G->A and T->A) in *Sufu*$^{Ex456(fl)/Ex456(fl)}$ cDNA. Exon/intron borders are indicated. (C) Schematic overview of the *Sufu*$^{Ex456(fl)}$ allele, displaying exons 4 through 8. Orange and green dotted lines indicate splicing events leading to exon 6 and exon 5–6 skipping, respectively. Red circles mark identified point mutations in intron 5. Blue and pink triangles indicate *frt* and *loxP* sites, respectively.

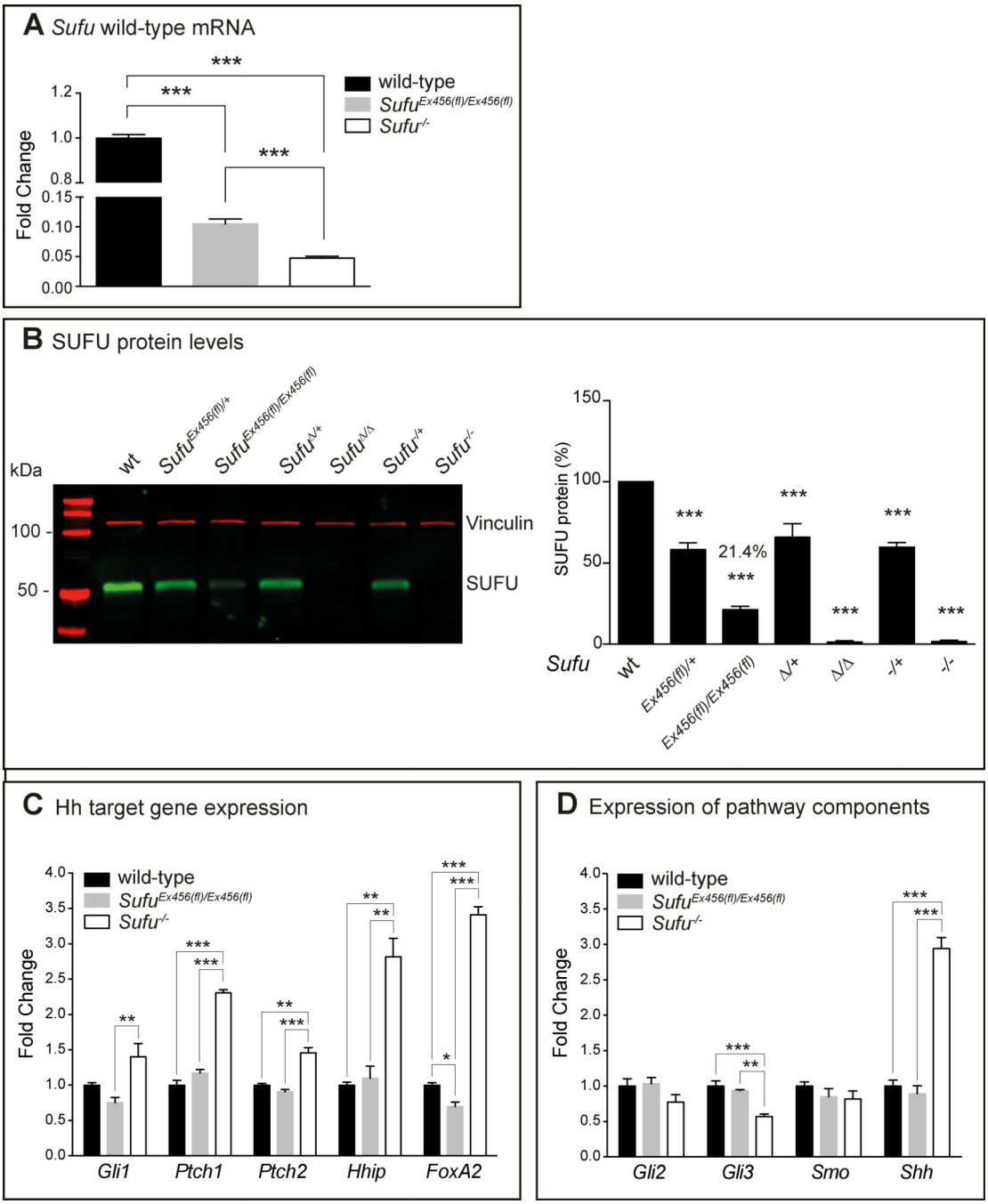

Fig. 3. Reduction of *Sufu* wild-type mRNA and protein does not result in increased HH target gene expression

(A) qRT-PCR comparing *Sufu* wild-type mRNA expression in wild-type, $Sufu^{Ex456(fl)/Ex456(fl)}$ and $Sufu^{-/-}$ E9.5 embryos. Data are expressed as mean values ± SEM of three independent experiments; *** p≤ 0.001, One-way ANOVA. wt, wild-type. (B) Western blot and quantification of SUFU protein levels in E9.5 embryos of indicated genotypes. Bar graph shows data normalized to control and expressed as percentage relative to wild-type levels (set to 100%, except for the GLI3FL/GLI3R ratio). Data are shown as mean values ± SEM of four independent experiments; *** p≤ 0.001, One-way ANOVA. wt,

wild-type. (C) qRT-PCR analysis of the hedgehog pathway target gene expression and (D) expression of *Gli2*, *Gli3*, *Smo* and *Shh* in $Sufu^{Ex456(fl)/Ex456(fl)}$, $Sufu^{-/-}$ and wild-type E9.5 embryos. Data are expressed as mean values ± SEM of three independent experiments; * $p \leq 0.05$, ** $p \leq 0.01$, *** $p \leq 0.001$, One-way ANOVA.

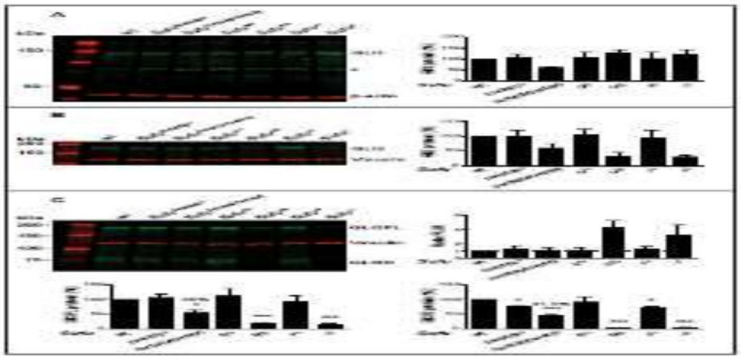

Fig. 4. Diminished levels of GLI proteins in *Sufu*$^{Ex456(fl)/Ex456(fl)}$ embryos

Western blot and quantification of GLI1 (A), GLI2 (B), and GLI3 (C) protein levels in E9.5 embryos of indicated genotypes. Bar graphs show quantification of GLI proteins as well as the ratio of GLI3FL and GLI3R. Data are normalized to control and expressed as percentage relative to wild-type levels (set to 100%). Dashed line indicates a ratio of 1. Data are expressed as mean values ± SEM of three or four independent experiments; * $p \leq 0.05$, *** $p \leq 0.001$, One-way ANOVA. # denotes unspecific bands. wt, wild-type.

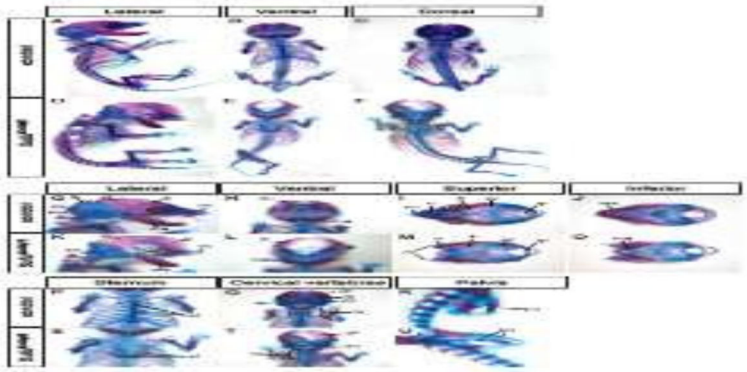

Fig. 5. Severe skeletal malformations in *Sufu*$^{Ex456(fl)/Ex456(fl)}$ embryos

(A–F) Lateral, ventral and dorsal view of E18.5 control and *Sufu*$^{Ex456(fl)/Ex456(fl)}$ embryos stained with alcian blue and alizarin red to detect cartilage and bone, respectively. Asterisks indicate branching ribs. (G–U) Detailed view of the skull, vertebrae and pelvic abnormalities in *Sufu*$^{Ex456(fl)/Ex456(fl)}$ embryos. cv, cervical vertebrae; eo, exoccipital; fr, frontal; ip, interparietal; ma, mandibles; n, nasal; nc, nasal capsule; pr, parietal; pu, pubic bone; so, supraoccipital; st, sternum.

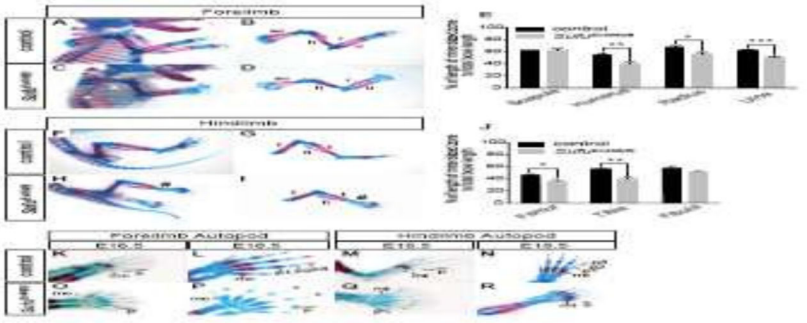

Fig. 6. *Sufu*$^{Ex456(fl)/Ex456(fl)}$ embryos exhibit reduced limb ossification

Alcian blue and alizarin red staining visualizing cartilage and bone, respectively. (A–D) Fore- and (F–I) hindlimbs of E18.5 control and *Sufu*$^{Ex456(fl)/Ex456(fl)}$ embryos. f, femur; fi, fibula; h, humerus; r, radius; sc, scapula; t, tibia; u, ulna. # indicates plantar flexion. (E, J) Bar graphs displaying % of length of mineralized bone to total bone length; (mean values ± SEM; n=4 embryos per group). * p≤ 0.05, ** p≤ 0.01, *** p≤ 0.001, t-test. (K–R) Detailed comparison between E16.5 and E18.5 fore- and hindlimb autopods of control and *Sufu*$^{Ex456(fl)/Ex456(fl)}$ embryos. p, phalanges; mc, metacarpals; mt, metatarsal; p1 proximal phalanges; p2, intermediate phalanges; p3, distal phalanges. White asterisks indicate branching ribs and black asterisks denote distal phalanges of Sufu$^{Ex456(fl)/Ex456(fl)}$ forelimb autopod.

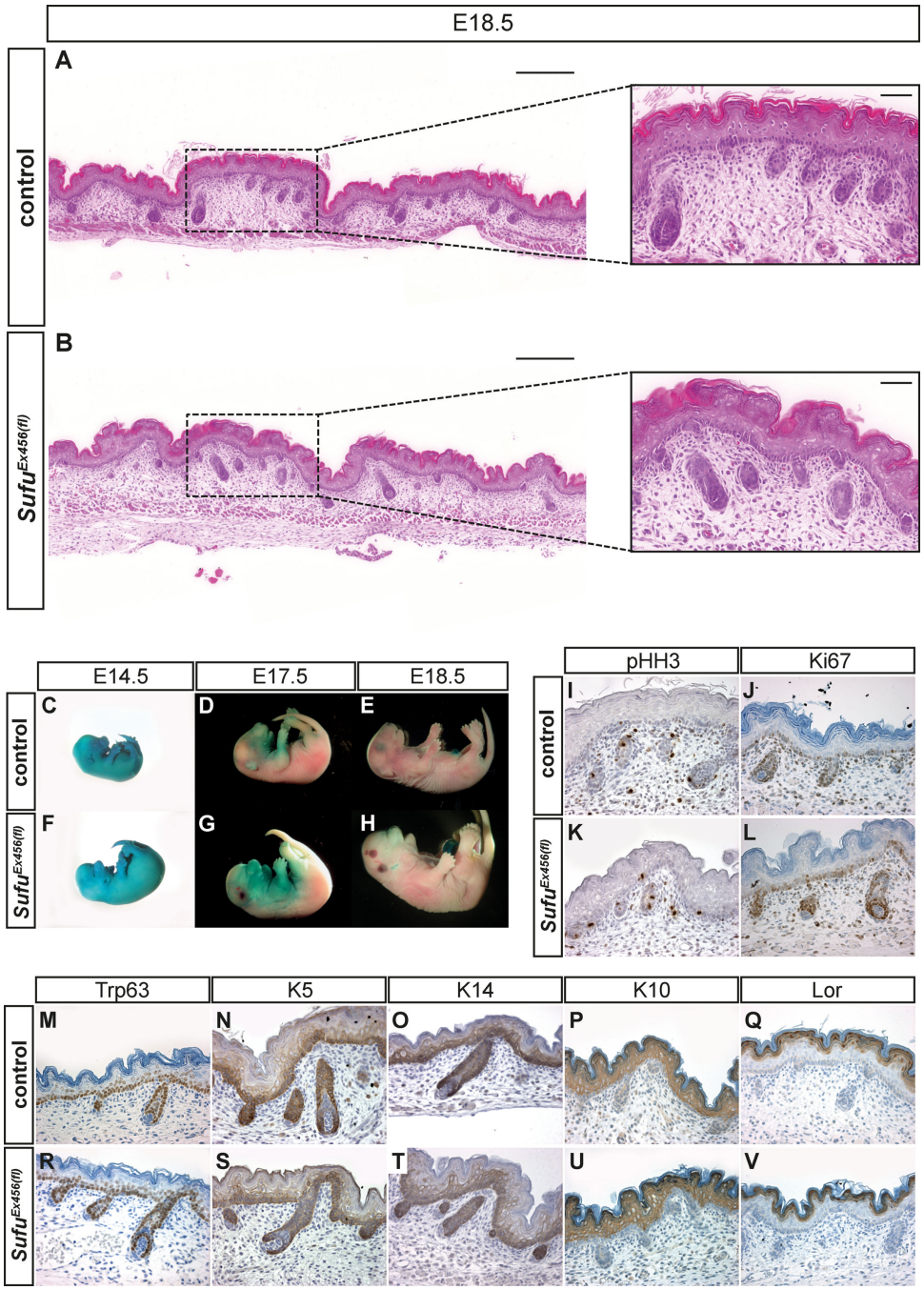

Fig. 7. Normal skin development *Sufu*$^{Ex456(fl)/Ex456(fl)}$ embryos

(A, B) Hematoxylin and eosin stained sections from E18.5 control and skin from *Sufu*$^{Ex456(fl)/Ex456(fl)}$ mice. Scale bar, 200μm. Insets show higher magnification (scale bar, 50μm). (C–H) Skin permeability assay using X-gal staining on control and *Sufu*$^{Ex456(fl)/Ex456(fl)}$ embryos of indicated ages. Blue staining indicates permeable skin. (I–V) Immunohistochemical staining for proliferation and epidermal markers in E18.5 skin of indicated genotype. pHH3, phospho-Histone H3; K5, Keratin 5; K14, Keratin 14; K10, Keratin 10; Lor, Loricrin. Objective used, 40x.

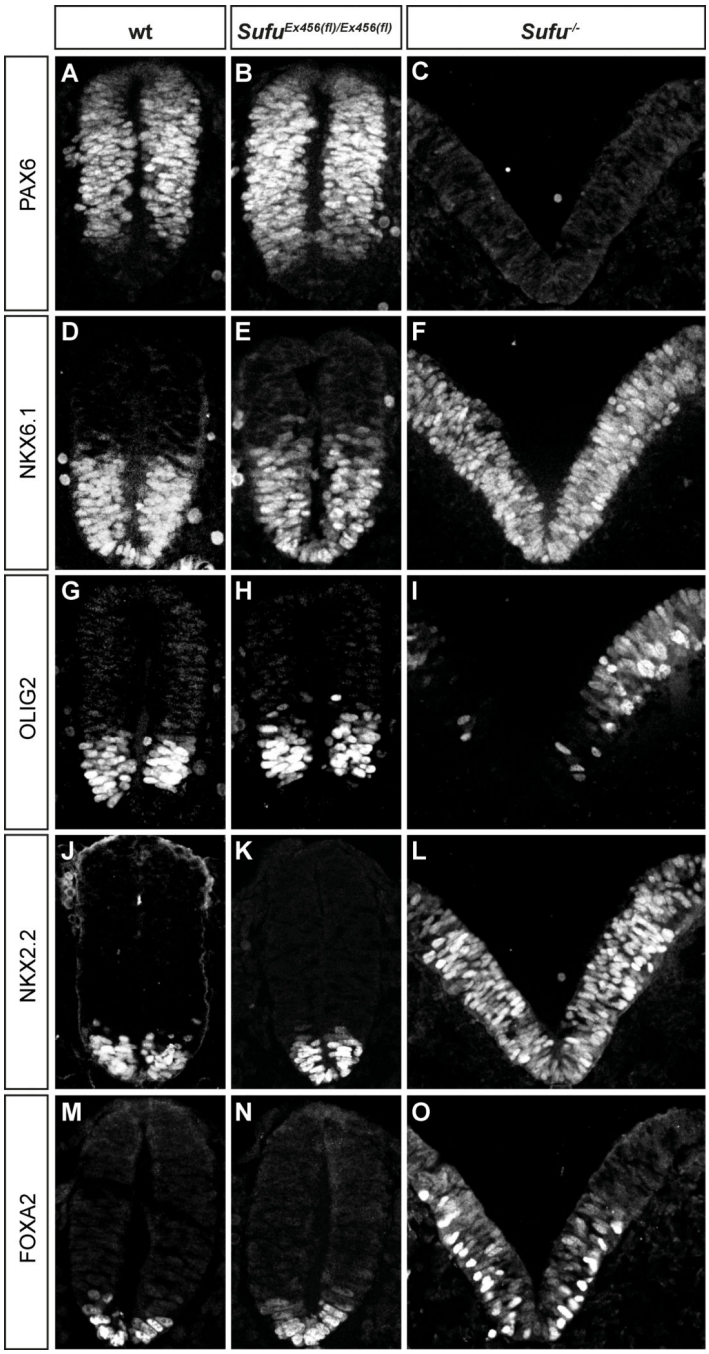

Figure 8. Patterning of the *Sufu*$^{Ex456(fl)/Ex456(fl)}$ neural tube is not altered

(A–O) Transverse sections of wild-type, *Sufu*$^{Ex456(fl)/Ex456(fl)}$ and *Sufu*$^{-/-}$ E9.0 neural tubes stained with antibodies against PAX6 (A–C), NKX6.1 (D–F), OLIG2 (G–I), NKX2.2 (J–L) and FOXA2 (M–O).

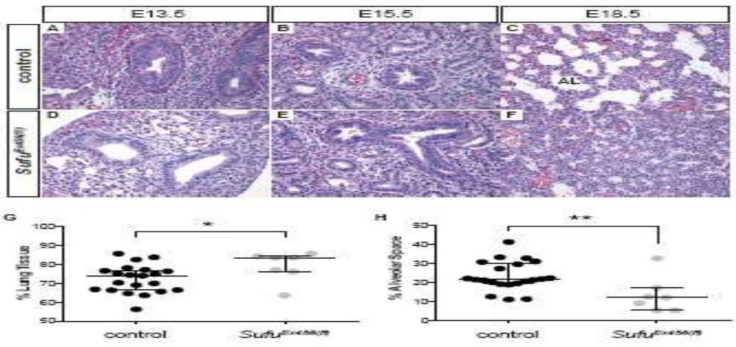

Figure 9. Abnormal lung development in *Sufu*$^{Ex456(fl)/Ex456(fl)}$ embryos

(A–F) Hematoxylin and eosin stained sections from control and *Sufu*$^{Ex456(fl)/Ex456(fl)}$ lungs at indicated embryonic stages. AL, alveolus. Objective used, 40x. (G) Quantification of % lung tissue and (H) % alveolar space of E18.5 control (n=21) and *Sufu*$^{Ex456(fl)/Ex456(fl)}$ (n=7) lungs. * $p \leq 0.05$, ** $p \leq 0.01$, t-test.